ACS APPLIED ENERGY MATERIALS

Article

Cite This: ACS Appl. Energy Mater. 2018, 1, 4626−4634

www.acsaem.org

Drastic Improvement of Air Stability in an n-Type Doped Naphthalene-Diimide Polymer by Thionation

Diego Nava,[†,‡] Younghun Shin,[§] Matteo Massetti,[†,‡] Xuechen Jiao,[∥,⊥] Till Biskup,[#] Madan S. Jagadeesh,[‡] Alberto Calloni,[‡] Lamberto Duò,[‡] Guglielmo Lanzani,[†,‡] Christopher R. McNeill,[∥] Michael Sommer,*[,§] and Mario Caironi*[,†]

[†]Center for Nano Science and Technology @PoliMi, Istituto Italiano di Tecnologia,, Via Pascoli 70/3, Milano 20133, Italy

[‡]Dipartimento di Fisica, Politecnico di Milano, Piazza L. da Vinci 32, Milano 20133, Italy

[§]Institut für Chemie, Technische Universität Chemnitz, Straße der Nationen 62, Chemnitz 09111, Germany

[∥]Department of Materials Science and Engineering, Monash University, Wellington Road, Clayton, Victoria 3800, Australia

[⊥]Australian Synchrotron, 800 Blackburn Road, Clayton, Victoria 3168, Australia

[#]Institut für Physikalische Chemie, Albert-Ludwigs-Universität Freiburg, Albertstraße 21, 79104 Freiburg, Germany

Supporting Information

ABSTRACT: Organic thermoelectrics are attractive for the fabrication of flexible and cost-effective thermoelectric generators (TEGs) for waste heat recovery, in particular by exploiting large-area printing of polymer conductors. Efficient TEGs require both p- and n-type conductors: so far, the air instability of polymer n-type conductors, which typically lose orders of magnitude in electrical conductivity (σ) even for short exposure time to air, has impeded processing under ambient conditions. Here we tackle this problem in a relevant class of electron transporting, naphthalene-diimide copolymers, by substituting the imide oxygen with sulfur. n-type doping of the thionated copolymer gives rise to a higher σ with respect to the non-thionated one, and most importantly, owing to a reduced energy level of the lowest-unoccupied molecular orbital, σ is substantially stable over 16 h of air exposure. This result highlights the effectiveness of chemical tuning to improve air stability of n-type solution-processable polymer conductors and shows a path toward ambient large-area manufacturing of efficient polymer TEGs.

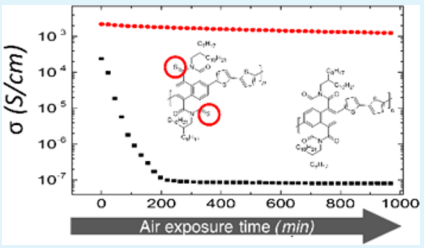

KEYWORDS: *polymer conductors, n-type doping, organic thermoelectrics, air stability, conjugated polymers*

INTRODUCTION

Energy harvesting with organics sees its most mature example in organic solar cells, which enable lightweight and large-area solar energy converters suitable for distributed energy generation.[1,2] Organic materials could also support the development of other energy harvesting and scavenging[3] devices that necessitate cost-competitive technologies to be economically viable, such as thermoelectric generators (OTEGs), that could be employed to supply power to low-consumption distributed and/or portable electronic devices. At the same time, such development could lead to custom-shaped active coolers,[4,5] facilitating their integration into existing electronic appliances. One of the most appealing paths toward such applications is to make use of solution-processed organic compounds in order to enable mass-printed OTEGs, thus drastically limiting production costs. Yet, the development of organic thermoelectrics is far less mature than photovoltaics, with critical shortfalls in fundamental knowledge regarding the thermoelectric properties of conjugated molecule-based films,[6,7] available materials,[8−10] processing,[11−13] and device engineering.[14−18]

The efficiency of the conversion of a heat flux into a current by thermoelectric (TE) materials can be related to the dimensionless material figure of merit zT, defined as

$$zT = \frac{S^2\sigma}{\kappa}T \quad (1)$$

where σ is the electrical conductivity, S is the Seebeck coefficient, and κ is the thermal conductivity.

One of the most attractive characteristics of organic conductors or doped organic semiconductors is their low κ, typically below 1 W m^{-1} K^{-1},[9,19] as a result of the suppression of the phonon component in the thermal conductivity due to the intrinsic structural disorder.[20] A common strategy therefore to improve TE properties of organic semiconductors is to improve the numerator of zT, namely, the power factor (PF).

$$PF(\mathrm{W\,m^{-1}\,K^{-2}}) = S^2\sigma \quad (2)$$

Received: May 16, 2018
Accepted: August 14, 2018
Published: August 14, 2018

DOI: 10.1021/acsaem.8b00777
ACS Appl. Energy Mater. 2018, 1, 4626−4634

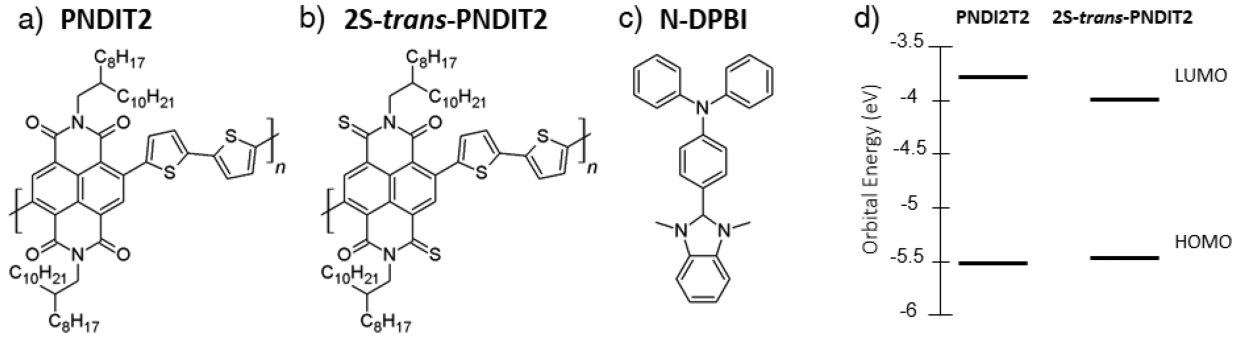

Figure 1. Chemical structures of (a) PNDIT2, (b) thionated derivative 2*S*-*trans*-PNDIT2, and (c) hydride dopant *N*-DPBI. (d) Energy diagram for frontier energy orbitals of both copolymers obtained from cyclic voltammetry and absorption in solution.

Since in their pristine form conjugated organic materials are typically insulators or semiconductors with low background conductivity, doping is necessary to achieve suitable electrical conductivity.[21] Thus, tuning the doping level, namely, modulating the charge carrier density, is a key aspect for optimizing *PF* and *zT* values.[22] In organic semiconductors the doping process relies on the addition of substoichiometric amounts of a redox-active species to the host semiconductor matrix. The dopant, which is a molecular species or a salt,[23,24] donates an electron to the host (n-doping) or accepts an electron from the host, leaving a hole behind (p-doping) as a consequence either of direct charge transfer[25−28] or of an indirect process. For example, proton transfer from acids or hydride transfer can lead to p-type and n-type doping, respectively.[29]

For the realization of an efficient thermoelectric device, complementary p-type and n-type conducting materials with high *PF* are needed at the same time.[30] While solution-processable organic p-type materials having a *PF* in excess of 100 μW m^{-1} K^{-2} have been demonstrated,[31−34] the major limitations are ascribable to n-type materials, for which examples combining high electrical conductivity and solution processability are very scarce. A further strong limitation for n-type materials arises from their air instability, which precludes ambient processing of OTEGs and imposes severe constraints regarding devices encapsulation.[35]

To overcome this issue, both the dopant and the semiconductor must be air-stable. With regard to the dopant, adopting species with very low ionization energy to induce an electron transfer to the host semiconductor is critical, because the donating molecule is very prone to redox reactions with species in the atmosphere.[36] This is the reason why the hydride transfer scheme proposed by Bao and co-workers from ambient stable benzimidazole derivatives, such as 4-(1,3-dimethyl-2,3-dihydro-1*H*-benzoimidazol-2-yl)-*N*,*N*-dimethylaniline (*N*-DMBI) and 4-(1,3-dimethyl-2,3-dihydro-1*H*-benzoimidazol-2-yl)-*N*,*N*-diphenylaniline (*N*-DPBI), immediately gained interest.[37] Chabinyc and co-workers reported a maximum conductivity of 10^{-3} S cm^{-1} for poly{[*N*,*N*′-bis(2-octyldodecyl)naphthalene-1,4,5,8-bis(dicarboximide)-2,6-diyl]-*alt*-5,5′-(2,2′-bithiophene)}, here abbreviated as PNDIT2 (Figure 1a), doped with *N*-DMBI.[38] Koster and co-workers[39,40] recently explored a benzimidazole derivative to dope a modified fullerene, both tailored with hydrophilic triethylene glycol type side chains, achieving an electrical conductivity of 2.05 S cm^{-1} and a *PF* of 19.1 μW m^{-1} K^{-2}, one of the highest reported for solution processable n-type materials. Pei and co-workers[41] reported a series of BDPPV n-type conjugated polymers with low-lying LUMO levels and very high *PF* values up to 28 μW m^{-1} K^{-2}. However, all the previous systems did not exhibit air stability or at least this aspect was not investigated. Generally, it is assumed that ambient stability of n-type conductivity can be achieved using materials with a LUMO energy level more negative than −3.9 eV.[42−46]

The lowering of the LUMO energy of the semiconductor can be obtained by diverse modifications of the electron withdrawing cores such as in naphthalene-diimide (NDI)-based copolymers, one of the most studied classes of n-type materials.[47−55] With the core positions being partially blocked in PNDIT2 by the co-monomer, the strategy of lowering the LUMO by replacing the imide group by a monothioimide group, known as thionation, appears highly suitable for the development of stable n-doped small molecule NDIs[56−59] and NDI-based polymers.[60,61]

Here we make use of thionated PNDIT2, referred to as 2*S*-*trans*-PNDIT2 (Figure 1b) in which two carbonyl oxygens are substituted by sulfur with full trans-regioselectivity.[61] 2*S*-*trans*-PNDIT2 exhibits a lower LUMO level compared to PNDIT2 which enables a drastically improved stability of n-type electrical conductivity at ambient conditions. When doped with *N*-DPBI (Figure 1c), σ is as high as 6×10^{-3} S cm^{-1}, with an improved power factor with respect to PNDIT2, reaching 4.9×10^{-2} μW m^{-1} K^{-2}. Importantly, while doped PNDIT2 films lose several orders of magnitude of σ within 200 min, reaching almost the low conductivity of the undoped film, the conductivity of 2*S*-*trans*-PNDIT2 decreases by only a factor of 2 after 16 h of continuous air exposure.

MATERIALS

The herein used 2*S*-*trans*-PNDIT2 was obtained from the educt PNDIT2 using Lawesson's reagent as previously published.[61] This PNDIT2 has a molecular weight from size exclusion chromatography (SEC), $M_{n,SEC}/M_{w,SEC}$ = 12/19 (kg/mol), and was also used as a reference herein. The molecular weight of 2*S*-*trans*-PNDIT2 obtained by SEC under the same conditions was $M_{n,SEC}/M_{w,SEC}$ = 8/355 (kg/mol). However, for an equal chain length of the two materials it is apparent that the molar mass of 2*S*-*trans*-PNDI must be slightly higher than that of the corresponding educt PNDIT2. In fact molar mass determination by SEC is not straightforward here, as also seen by the very high M_w values caused by aggregation. We therefore made additional use of NMR end group analysis, which gives a $DP_{n,NMR}$ of 8.7 for PNDIT2 (and the same value for 2*S*-*trans*-PNDIT2).[61] From the masses of the repeat units and an O/S conversion of 96% for 2*S*-*trans*-PNDIT2, we estimate absolute number-average molecular weights $M_{n,NMR}$,

DOI: 10.1021/acsaem.8b00777
ACS Appl. Energy Mater. 2018, 1, 4626−4634

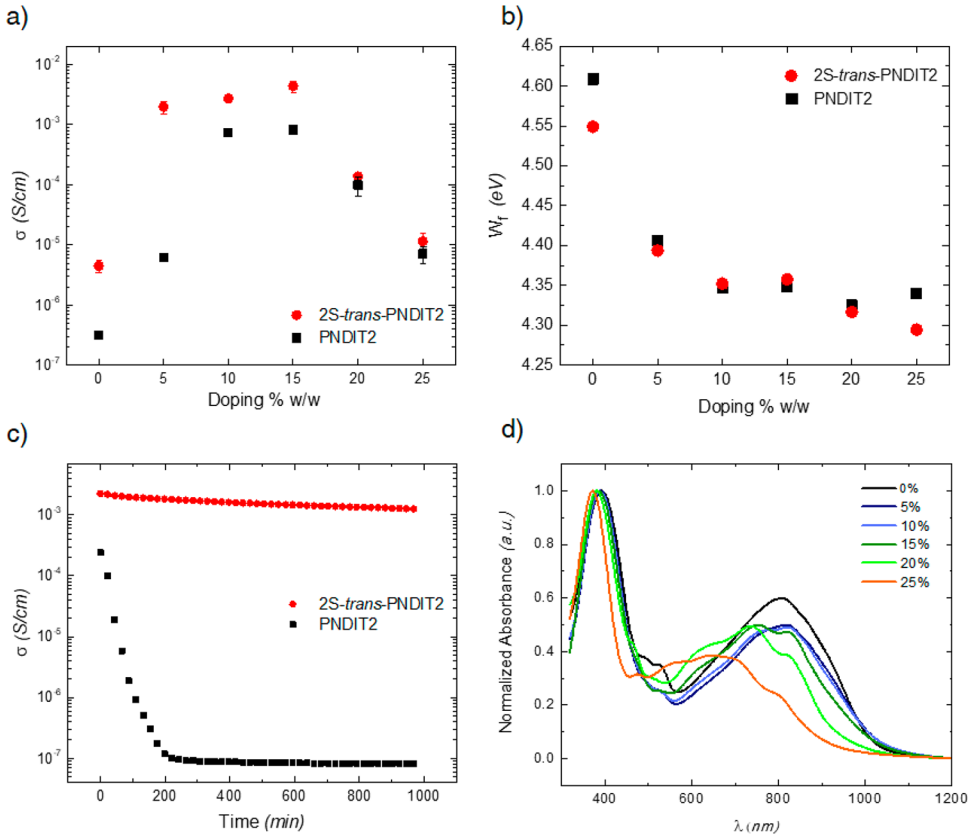

Figure 2. (a) Electrical conductivity of 2*S*-*trans*-PNDIT2 (red dots) and PNDIT2 (black squares) thin films as a function of the *N*-DPBI dopant concentration. Each data point is an average of at least four devices; vertical error bars represent the standard deviation. (b) Work function plot for 2*S*-*trans*-PNDIT2 (dots) and PNDIT2 (squares) as a function of doping concentration. (c) Time dependence of the electrical conductivity of non-encapsulated thin films of 2*S*-*trans*-PNDIT2 (red dots) and PNDIT2 (black squares), with 15% (w/w) *N*-DPBI, upon ambient air exposure. (d) UV−vis−near-IR thin film absorption spectra of 2*S*-*trans*-PNDIT2 doped with different w/w concentrations of *N*-DPBI.

of 8.6 and 8.9 kg/mol for PNDIT2 and 2*S*-*trans*-PNDIT2, respectively.

OPTICAL AND ELECTRICAL PROPERTIES

The effect of the substitution of the imide oxygen atoms with sulfur atoms is clearly visible from the UV−visible absorption spectra (see Supporting Information, SI, Figure S1).[61] Comparing the spectra of the PNDIT2 and 2*S*-*trans*-PNDI, a strong red shift of ≈100 nm in the absorption onset is observed for the latter, indicating a significant reduction of the optical energy gap. Since the HOMO is mostly located on the thiophene moieties,[62] while the LUMO is localized on the naphthalene-diimide unit,[63] the energy gap reduction should be ascribable to a deeper LUMO energy level as an effect of thionation. This is confirmed by cyclic voltammetry measurements (Figure S2), as reported by Shin et al.[61] By combining optical data and electrochemical data, following the methodology described in the SI, we can obtain a first estimation of the HOMO/LUMO energies (Figure 1d). For 2*S*-*trans*-PNDIT2 we extract energy values of −5.47 eV for the HOMO level and −3.96 eV for the LUMO, while for PNDIT2 we obtain −5.51 and −3.75 eV, respectively, for the HOMO and the LUMO levels. As expected, thionation of the acceptor moiety mostly reduces the LUMO level of 2*S*-*trans*-PNDIT2, while leaving the HOMO level substantially unperturbed.

In order to dope the polymer films, we selected *N*-DPBI. Following the procedure reported by Schlitz et al. for PNDIT2,[38] we added *N*-DPBI directly to the 2*S*-*trans*-PNDIT2 toluene solution at various concentrations, from 5% to 25% by weight, and deposited a 40 nm thick film by spin-coating. We applied the same doping procedure to PNDIT2 as a reference.

In its pristine, undoped state, the 2*S*-*trans*-PNDIT2 film shows an electrical conductivity of $(4 \pm 2) \times 10^{-6}$ S cm^{-1}. For undoped PNDIT2, a value that is 1 order of magnitude lower is found $(3 \pm 1) \times 10^{-7}$ S cm^{-1}. This is in agreement with electron spin resonance (ESR) spectroscopy data indicating the presence of unpaired electrons in 2*S*-*trans*-PNDIT2, but not in PNDIT2 (Figure S11). After the addition of only 5% (w/w) of *N*-DPBI, the conductivity of 2*S*-*trans*-PNDIT2 films drastically increases by more than 2 orders of magnitude, reaching $(2.0 \pm 0.1) \times 10^{-3}$ S cm^{-1}. An increase of the doping concentration above 5% (w/w) at first leads to a small increase of σ, reaching a maximum value of $(5.9 \pm 0.2) \times 10^{-3}$ S cm^{-1} at 15% (w/w) of *N*-DPBI. A further increase in dopant concentration is then detrimental for the electrical conductivity. A similar dependence of σ on dopant concentration was observed for PNDIT2 reference films, in good agreement with literature,[38,64−66] where the maximum σ of $(1.2 \pm 0.2) \times 10^{-3}$ S cm^{-1}, achieved at 15% (w/w), is five times lower than for 2*S*-*trans*-PNDIT2. The difference in σ between the two systems is much stronger at low doping concentration: at 5% (w/w), σ is 330 times higher in the thionated sample than in the parent copolymer, and even two times higher than the maximum electrical conductivity achieved at 15% (w/w) in PNDIT2.

DOI: 10.1021/acsaem.8b00777
ACS Appl. Energy Mater. 2018, 1, 4626−4634

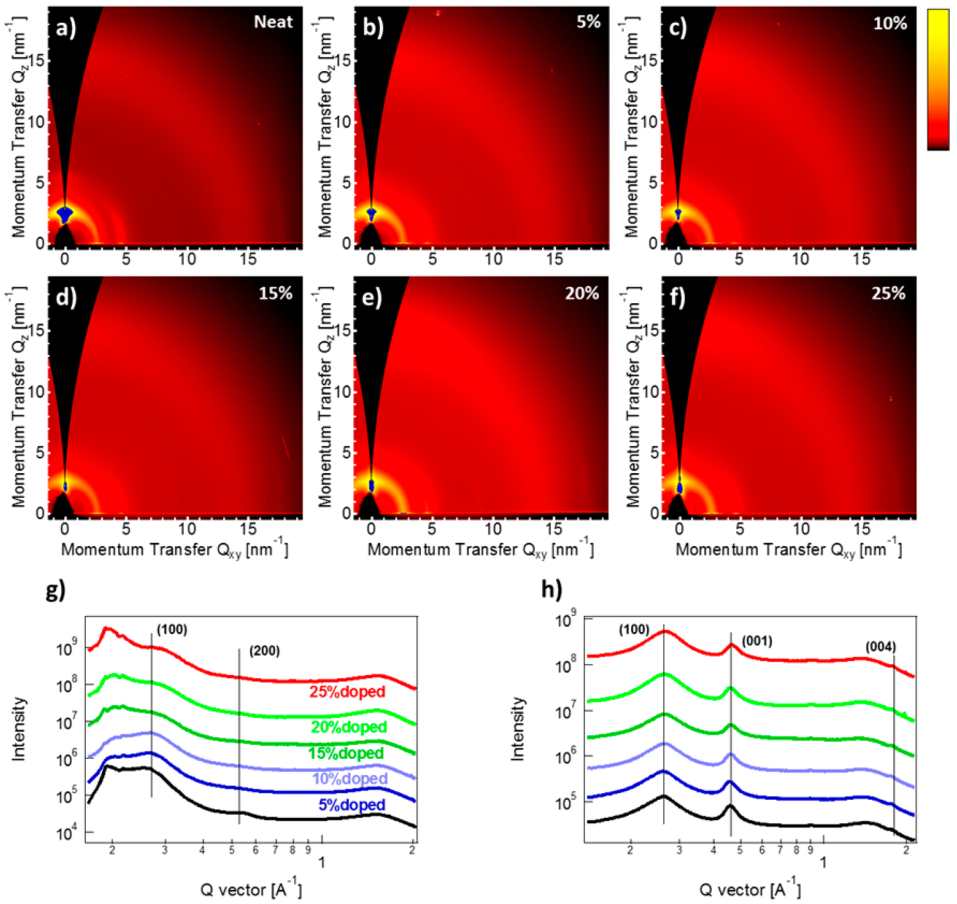

Figure 3. Two-dimensional data plots of GIWAXS measurements of 2*S*-*trans*-PNDIT2 films for different doping concentrations, from (a) to (f): 0, 5, 10, 15, 20, and 25% (w/w). Corresponding one-dimensional (g) out-of-plane and (h) in-plane GIWAXS profiles.

The effect of doping was also monitored by measuring the work function (W_f) by the Kelvin probe technique (Figure 2b). Undoped films of 2*S*-*trans*-PNDIT2 feature a lower W_f, in agreement with an increased number of excess electrons already seen with ESR. With increasing dopant concentration, W_f reduces from 4.55 eV in the pristine film to 4.35 eV in the doped film at 10% w/w concentration, where it reaches a plateau; a further increase in the doping concentration does not lead to an appreciable reduction of the work function as detectable by our Kelvin probe setup. X-ray photoemission spectroscopy (XPS) was used to certify the presence of dopant molecules and to assess their chemical state. In particular, in the case of doped 2*S*-*trans*-PNDIT2 films, we detected the spectroscopic features of oxidized *N*-DPBI molecules (Figure S4 in the Supporting Information and details therein).

Besides the difference in σ, what is remarkable is the difference in stability of the electrical conductivity between the two systems when films are directly exposed to ambient air. Figure 2c reports σ as a function of the ambient air exposure time, at room temperature and relative humidity of about 50%, for both materials at a doping concentration of 15% (w/w). The electrical conductivity of PNDIT2 rapidly drops, reaching almost the pristine film value after 200 min. Such strong instability basically prevents any ambient processing of this doped system and its use for OTEGs fabrication. On the contrary, the electrical conductivity of 2*S*-*trans*-PNDIT2 remains within the same order of magnitude of its initial value for as long as 16 h of air exposure, showing only a reduction factor slightly lower than 2. Similar behavior in air stability was observed in 2*S*-*trans*-PNDIT2 for 5% (w/w) and 10% (w/w) doping concentrations (Figure S10). We assign the enhanced stability to the lower LUMO level in 2*S*-*trans*-PNDIT2 that allows electrons to relax at energy levels less prone to redox processes in ambient air. This is an unprecedented stability for doped n-type organic materials and would clearly leave room for ambient processing of organic thermoelectric devices, strongly desirable in the case of high-throughput printing processes, before encapsulation.[46]

It is interesting to note that the field-effect mobility as measured in bottom-contact, top-gate field-effect transistors based on the pristine thin films, is higher for PNDIT2 than for 2*S*-*trans*-PNDIT2, reaching values of 0.30 ± 0.02 and 0.05 ± 0.01 $cm^2 V^{-1} s^{-1}$, respectively (details reported in Figure S5).[61] The bulk mobility of doped films and the mobility of field-effect transistors are not directly comparable.[67,68] However, since the charge density achieved in the field-effect device is of the same order of magnitude as the one achieved in doped films,[69,70] it is reasonable to expect that the higher conductivity in doped 2*S*-*trans*-PNDIT2 films (Figure 3a) is not caused by an improved electron mobility.

Thus, the improved σ in doped 2*S*-*trans*-PNDIT2 films suggests a higher efficacy of the doping process leading to a higher charge density. The ESR signal intensity for 2*S*-*trans*-PNDIT2 at 15% (w/w) doping was two times higher than the one of PNDIT2, clearly confirming a higher carrier density (Figure S12).

To further investigate the factors that cause the higher conductivity of 2*S*-*trans*-PNDIT2, we followed the doping

DOI: 10.1021/acsaem.8b00777
ACS Appl. Energy Mater. 2018, 1, 4626−4634

process through optical absorption and structural measurements on thin films as a function of doping concentration. Figure 2d shows the UV−vis optical absorption spectra evolution of 2*S*-*trans*-PNDIT2 with doping concentration. The pristine film has a broad band from 600 to 1000 nm, with a peak around 810 nm. The strong red shift with respect to the spectrum of molecularly dissolved chains in chloronaphthalene solution is due to aggregation.[62] At low doping concentration (5 and 10% (w/w)), the intensity of the low-energy band reduces, with the appearance of a stronger component at around 600 nm in the 10% (w/w) case, indicating an increased presence of a nonaggregated, amorphous phase. For a doping concentration above 15% (w/w), the shoulder between 800 and 1000 nm becomes increasingly suppressed in favor of the nonaggregated component at 600 nm and the ratio between the 750 and 830 nm peaks rapidly increases. Overall, the evolution of the UV−vis spectra with doping concentration suggests that the dopant molecule suppresses chain−chain interactions of 2*S*-*trans*-PNDIT2, resulting in an increased amorphous component. Differently, in the case of doped PNDIT2 (Figure S3), an increasing doping concentration mainly causes a reduction of the intensity of the 600−800 nm band while keeping the ratio of vibronic bands constant up to 15% (w/w). Higher doping concentrations did not lead to further modification of the UV−vis spectra, indicating a weaker interaction of the dopant with PNDIT2.

Optical absorption measurements therefore suggest a structural evolution in 2*S*-*trans*-PNDIT2 films with doping.

MORPHOLOGICAL CHARACTERIZATION

The microstructure of these thin films was further investigated by grazing incidence wide-angle X-ray scattering (GIWAXS). Comparing the GIWAXS patterns of films of undoped 2*S*-*trans*-PNDIT2 (Figure 3a) and PNDIT2 (Figure S4a), 2*S*-*trans*-PNDIT2 exhibits less microstructural order. Although lamellar packing and backbone repeat distance are similar, 2*S*-*trans*-PNDIT2 exhibits a lower degree of crystalline order evidenced by broader peaks with an apparent absence of a $\pi-\pi$ stacking peak.[61] Furthermore, films of 2*S*-*trans*-PNDIT2 exhibit more orientational disorder, with crystallites exhibiting broad orientational distributions from face-on to edge-on. Thus, thionation of PNDIT2 reduces microstructural order which may explain in part the reduced field-effect mobilites of 2*S*-*trans*-PNDIT2 compared to PNDIT2.[61] With increasing doping concentration, 2*S*-*trans*-PNDIT2 displays a further decrease in order. Undoped films (Figure 3a), while exhibiting a range of molecular orientations, show a slight preference for edge-on orientation, evidenced by the first-order lamellar stacking peak, (100), at ∼2.5 nm^{-1} along the out-of-plane direction, with a second-order peak, (200), also observable at ∼5 nm^{-1} (see also in-plane traces in Figure 3g). With increased doping, this edge-on population is less evident, with no preference for face-on or edge-on orientation in films with 15% (w/w) doping and above. The lamellar stacking *d*-spacings for the remaining crystalline population appear unaffected (Figure 3h), indicating that the dopant molecule is not intercalating within the side chains. Since a $\pi-\pi$ stacking peak is not clearly present, it is not possible to say whether the dopant molecules are intercalating between two stacked backbones. A strikingly different behavior with doping is observed for the parent PNDIT2 (Figure S6). As-cast PNDIT2 films exhibit a pronounced edge-on stacking of chains, with four orders of lamellar stacking peaks evident. We note that this is unusual for PNDIT2 films, likely due to the low molecular weight adopted in this case. With doping, PNDIT2 appears to become more ordered, evidenced by narrower lamellar stacking and backbone peaks, unlike for 2*S*-*trans*-PNDIT2, where the doping induces more structural disorder. Similar to 2*S*-*trans*-PNDIT2, the observed *d*-spacings are unaffected by doping, indicating that the dopant is not intercalating within the crystals. In both cases no scattering from the dopant crystals is appearing, with the second-order lamellar stacking no longer evident.

Taking together the results from optical absorption and GIWAXS, we conclude that *N*-DPBI dopant is predominantly incorporated in the amorphous portion of 2*S*-*trans*-PNDIT2 films and does not substantially alter the molecular packing motif of the crystals that do form. Since 2*S*-*trans*-PNDIT2 features less microstructural order, miscibility with *N*-DPBI is likely increased. Addition of *N*-DPBI thus hinders the crystallization of 2*S*-*trans*-PNDIT2, in a fashion similar to the way fullerene molecules such as PCBM hinder the crystallization of poly(3-hexylthiophene) in as-cast P3HT/PCBM blends.[71] A higher 2*S*-*trans*-PNDIT2 amorphous fraction in blends with *N*-DPBI is consistent with the appearance of a nonaggregated absorption component in UV−vis spectra with increasing dopant concentration. A reduction in the extension of polymer crystallites upon dopant addition results in a smaller fraction of the film which is precluded to the dopant and can explain the higher conductivity at 5% (w/w) doping with respect to PNDIT2, despite a lower field-effect mobility. Still, at high dopant concentration, miscibility of the two components is a limiting factor on the doping efficacy, with an obvious phase separation, also evidenced by AFM topography measurements (Figure S7).[38] For PNDIT2 films, the high tendency of PNDIT2 chains to crystallize means that there is a lower fraction of chains which are able to interact with the dopant on the molecular level.

SEEBECK MEASUREMENTS

The Seebeck coefficient of the two doped copolymers was finally measured at 15% (w/w). For 2*S*-*trans*-PNDIT2 thin films doped with *N*-DPBI at 15% (w/w), we obtained $S = -90 \pm 4\ \mu V\ K^{-1}$, leading to a power factor of $4.9 \times 10^{-2}\ \mu W\ m^{-1}\ K^{-2}$. The negative sign of the Seebeck is indicative of electrons being the majority carriers. *PF* is significantly higher than the maximum value we can obtain with PNDIT2, where we extract $PF = 1.2 \times 10^{-2}\ \mu W\ m^{-1}\ K^{-2}$ under the same conditions, in line with the results reported by Wang et al.[64] Thus, thionation of PNDIT2 is not only effective in drastically improving the air stability of doped NDI-based copolymer films but also in improving the overall thermoelectric performance. The improved electrical conductivity, owing to a more favorable interaction of the dopant and the polymer, enables a 4-fold improvement in power factor to be realized.

CONCLUSIONS

In conclusion, we have reported an effective strategy to strongly improve ambient stability of n-type doped NDI-based copolymers. The lower LUMO level of 2*S*-*trans*-PNDIT2 reduces the reactivity of excess electrons in air significantly. 2*S*-*trans*-PNDIT2 also has a weaker tendency to crystallize compared to PNDIT2, which promotes favorable molecular interactions between the polymer backbone and the dopant.

DOI: 10.1021/acsaem.8b00777
ACS Appl. Energy Mater. 2018, 1, 4626−4634

Doping of 2*S*-*trans*-PNDIT2 with the stable *N*-DPBI molecule produces a strong increase of electrical conductivity already at a doping concentration as low as 5% (w/w), and the *PF* extracted at maximum σ is four times higher than PNDIT2. The stability of σ for doped 2*S*-*trans*-PNDIT2 films completely exposed to air is unprecedented for n-type conductivity in polymers. 2*S*-*trans*-PNDIT2 shows a reduction in conductivity of less than a factor of 2 over 16 h of continuous air exposure, compared to the 3 orders of magnitude loss measured in the first hour only for PNDIT2. Such a pronounced improvement demonstrates that inherent environmental stability of n-type doped polymer conductors can be largely controlled through the proper design of the conjugated semiconductor system. This result is an important step toward stable n-type doped polymers, which more favorably allow ink formulation for large-area manufacturing through scalable printing technologies, which finally may enable high-throughput fabrication of low-cost and efficient organic thermoelectric generators under ambient conditions based on thermocouples combining n-type and p-type materials.

EXPERIMENTAL SECTION

Materials. PNDIT2 and 2*S*-*trans*-PNDIT2 were synthesized according to published procedures.[61,62] *N*-DPBI (4-(1,3-dimethyl-2,3-dihydro-1*H*-benzoimidazol-2-yl)-*N*,*N*-diphenylaniline) was purchased from Sigma-Aldrich and used as received.

Solutions Preparation. Both copolymers were dissolved in toluene at a concentration of 5 g/L and stirred at 80 °C for 4 h. *N*-DPBI solutions were prepared at concentrations of 3, 5, and 8 g/L and used after ≈12 h of dissolution at room temperature. Aliquots of polymer and dopant solution were mixed and stirred for 10 min at room temperature just before the deposition.

Thin Films Preparation. Low-alkali 1737F Corning glass was used as substrate. The substrates were cleaned in an ultrasonic bath of Milli-Q water, acetone, and isopropyl alcohol, 10 min for each step, and exposed to O_2 plasma at 100 W for 10 min. Electrodes were obtained by thermal evaporation, through a shadow mask, of a 1.5 nm thick Cr adhesion layer and 25 nm thick Au film. For field-effect transistors, bottom electrodes were patterned by a lift-off photolithographic process, defining a 20 μm channel length and a 2 mm channel width. Metals were deposited by thermal evaporation: 1.5 nm thick Cr, as adhesion layer and 20 nm thick Au. Thin polymer films were spin-cast from solutions onto prepatterned substrates, in a nitrogen-filled glovebox at 1000 rpm for 60 s and annealed at 150 °C for 2 h in inert atmosphere. For field-effect-transistor devices after the polymer thin film deposition, a dielectric layer with thickness of 600 nm was obtained by spin-coating an 80 g/L PMMA solution in *n*-butyl acetate at 1300 rpm for 60 s under nitrogen atmosphere, followed by an annealing at 80 °C for 1 h in inert atmosphere. The 40 nm thick gate contact was obtained by thermal evaporation of Al through a shadow mask.

Electrical Characterization. The *I*−*V* curves and the FET characteristics were measured at room temperature in N_2 atmosphere or in ambient air, Figure 2c, on a Wentworth Laboratories probe station with a semiconductor device analyzer (Agilent B1500A). The electrical conductivity was extracted through the linear fit of the *I*−*V* characteristics, Figure S8. The saturation mobility values were extracted using the gradual-channel approximation.

UV−Vis−Near-IR measurements. UV−vis−near-IR measurements were carried out on a PerkinElmer λ1050 spectrophotometer, using a tungsten lamp as source.

Kelvin Probe Measurements. Kelvin probe measurements were done in air with a KP Technology Ambient air Kelvin probe instrument. For the extraction of the work function we used the multiple single-point measurements mode. The work function of the sample was obtained by adding to the measured work function value the contact potential difference (CDP) of the tip, determined with an initial calibration on standard gold substrate.

ESR Measurements. Films were prepared under inert atmosphere by drop-casting 20 μL of solution (concentration of 5 g/L) onto synthetic quartz glass substrates (Ilmasil PS, QSIL GmbH) with dimensions of 3 × 25 mm^2, followed by annealing at 150 °C for 120 min after films were dried completely. The annealed films were placed into synthetic quartz glass tubes (Ilmasil PS, QSIL GmbH) with 3.8 mm outer and 3.0 mm inner diameters and the tubes sealed afterward. ESR spectra were recorded at room temperature on an Elexsys 580 (Bruker Biospin GmbH) spectrometer equipped with a 4119HS-W1 (Bruker) cavity: microwave frequency, 9.800 GHz; microwave power, 150 μW (30 dB attenuation, 150 mW source power); modulation frequency, 100 MHz; modulation amplitude, 0.1 mT.

GIWAXS Characterization. Grazing-incidence wide-angle X-ray scattering (GIWAXS) was performed at the SAXS/WAXS beamline at the Australian Synchrotron.[72] A set of 11 keV photons was used with scattering patterns recorded on a Dectris Pilatus 1 M detector. Images shown were acquired at an incident angle close the critical angle. Such images were chosen from a series of recorded 2D patterns with incident X-ray angle varying from 0.05° to 0.25° in the step of 0.01°. The X-ray exposure time was 1 s such that no film damage was identified. The sample-to-detector distance was calibrated using a silver behenate sample. The results were analyzed by an altered version of the NIKA 2D[73] based in IgorPro.

Atomic Force Microscopy. AFM polymer thin film samples were prepared using the same procedure described earlier in the Experimental Section. The surface morphology of the films was obtained with an Agilent 5500 atomic force microscope operated in the acoustic mode.

Seebeck Measurements. For the Seebeck measurements we employed a homemade setup described by Beretta et al.[74] The measurements were done under vacuum, at 10^{-4} mbar, to avoid convection phenomena and to preserve the polymer electrical properties. In addition, the measurements were performed at a temperature of 45 °C, to have an electrical resistance below 10 MΩ, which is our system threshold for a correct measurement of the Seebeck coefficient. Before the measurement, we annealed overnight the samples at 90 °C, to avoid any possible thermal effects and/or thermal hysteresis during the thermoelectric measurements.

ASSOCIATED CONTENT

Supporting Information

The Supporting Information is available free of charge on the ACS Publications website at DOI: 10.1021/acsaem.8b00777.

Optical and electrochemical characterization of both copolymers, extraction procedure of HOMO and LUMO levels, XPS analysis, field effect transistors characterization, GIWAXS characterization of PNDIT2, AFM images, current/voltage plots, and ESR spectra (PDF)

AUTHOR INFORMATION

Corresponding Authors

*(M.C.) E-mail: mario.caironi@iit.it.

*(M.S.) E-mail: michael.sommer@chemie.tu-chemnitz.de.

ORCID

Till Biskup: 0000-0003-2913-0004

Christopher R. McNeill: 0000-0001-5221-878X

Michael Sommer: 0000-0002-2377-5998

Mario Caironi: 0000-0002-0442-4439

Notes

The authors declare no competing financial interest.

DOI: 10.1021/acsaem.8b00777
ACS Appl. Energy Mater. 2018, 1, 4626−4634

■ ACKNOWLEDGMENTS

We thank F. Scuratti for help with AFM measurements. M.C. and D.N. acknowledge the European Research Council (ERC) for financial support, under the European Union's Horizon 2020 research and innovation programme "HEROIC", Grant Agreement 638059. Y.S. and M.S. acknowledge the Deutsche Forschungsgemeinschaft (Grant SO 1213/8-1) for funding. T.B. acknowledges the Deutsche Forschungsgemeinschaft (Grant BI 1249/3-1) for funding. This work was performed in part at the SAXS/WAXS beamline at the Australian Synchrotron, part of ANSTO. C.R.M. acknowledges support from the Australian Research Council (Grant DP170102145).

■ REFERENCES

(1) Huang, Y.; Kramer, E. J.; Heeger, A. J.; Bazan, G. C. Bulk Heterojunction Solar Cells: Morphology and Performance Relationships. *Chem. Rev.* **2014**, *114*, 7006−7043.
(2) Mazzio, K. A.; Luscombe, C. K. The Future of Organic Photovoltaics. *Chem. Soc. Rev.* **2015**, *44*, 78−90.
(3) LeBlanc, S. Thermoelectric Generators: Linking Material Properties and Systems Engineering for Waste Heat Recovery Applications. *Sustain. Mater. Technol.* **2014**, *1-2*, 26−35.
(4) Bahk, J.-H.; Fang, H.; Yazawa, K.; Shakouri, A. Flexible Thermoelectric Materials and Device Optimization for Wearable Energy Harvesting. *J. Mater. Chem. C* **2015**, *3*, 10362−10374.
(5) Zhao, D.; Tan, G. A Review of Thermoelectric Cooling: Materials Modeling and Applications. *Appl. Therm. Eng.* **2014**, *66*, 15.
(6) Zhang, Q.; Sun, Y.; Xu, W.; Zhu, D. What To Expect from Conducting Polymers on the Playground of Thermoelectricity: Lessons Learned from Four High-Mobility Polymeric Semiconductors. *Macromolecules* **2014**, *47*, 609.
(7) Culebras, M.; Gómez, C. M.; Cantarero, A. Review on Polymers for Thermoelectric Applications. *Materials* **2014**, *7*, 6701−6732.
(8) Sun, Y.; Sheng, P.; Di, C.; Jiao, F.; Xu, W.; Qiu, D.; Zhu, D. Organic Thermoelectric Materials and Devices Based on p - and n -Type Poly (Metal 1, 1, 2, 2-Ethenetetrathiolate) S. *Adv. Mater.* **2012**, *24*, 932−937.
(9) Yan, H.; Sada, N.; Toshima, N. Thermal Transporting Properties of Electrically Conductive Polyaniline Films as Organic Thermoelectric Material. *J. Therm. Anal. Calorim.* **2002**, *69*, 881−887.
(10) Kroon, R.; Kiefer, D.; Stegerer, D.; Yu, L.; Sommer, M.; Müller, C. Polar Side Chains Enhance Processability, Electrical Conductivity and Thermal Stability of a Molecularly p-Doped Polythiophene. *Adv. Mater.* **2017**, *29*, 1700930.
(11) Kiefer, D.; Yu, L.; Fransson, E.; Gómez, A.; Primetzhofer, D.; Amassian, A.; Campoy-quiles, M.; Müller, C. A Solution-Doped Polymer Semiconductor: Insulator Blend for Thermoelectrics. *Adv. Sci. news* **2017**, *4*, 1600203.
(12) Hong, C. T.; Kang, Y. H.; Ryu, J.; Cho, S. Y.; Jang, K. Spray-Printed CNT/P3HT Organic Thermoelectric Films and Power Generators. *J. Mater. Chem. A* **2015**, *3*, 21428−21433.
(13) Glaudell, A. M.; Cochran, J. E.; Patel, S. N.; Chabinyc, M. L. Impact of the Doping Method on Conductivity and Thermopower in Semiconducting Polythiophenes. *Adv. Energy Mater.* **2015**, *5*, 1401072.
(14) Park, T.; Park, C.; Kim, B.; Shin, H.; Kim, E. Environmental Science Power Factors to Generate Electricity by the Touch of Fingertips. *Energy Environ. Sci.* **2013**, *6*, 788−792.
(15) Lee, S. H.; Park, H.; Kim, S.; Son, W.; Cheong, I. W.; Kim, J. H. Transparent and Flexible Organic Semiconductor Nano Films with Enhanced Thermoelectric Efficiency. *J. Mater. Chem. A* **2014**, *2*, 7288−7294.
(16) Rojas, J. P.; Singh, D.; Conchouso, D.; Arevalo, A.; Foulds, I. G.; Hussain, M. M. Stretchable Helical Architecture Inorganic-Organic Hetero Thermoelectric Generator. *Nano Energy* **2016**, *30*, 691−699.
(17) Menon, A. K.; Yee, S. K. Design of a Polymer Thermoelectric Generator Using Radial Architecture. *J. Appl. Phys.* **2016**, *119*, No. 055501.
(18) Søndergaard, R. R.; Hosel, M.; Espinosa, N.; Jørgensen, M.; Krebs, F. C. Practical Evaluation of Organic Polymer Thermoelectrics by Large-Area R2R Processing on Flexible Substrates. *Energy Sci. Eng.* **2013**, *1*, 81−88.
(19) Zhang, X.; Lu, X.; Zhen, Y.; Liu, J.; Dong, H.; Zhao, G.; He, P.; Wang, Z.; Jiang, L.; Hu, W. Synthesis and Aggregation-Induced Emissions of Thienyl Substituted Cyclobutene Derivatives. *J. Mater. Chem. C* **2014**, *2*, 5083.
(20) Bubnova, O.; Khan, Z. U.; Malti, A.; Braun, S.; Fahlman, M.; Berggren, M.; Crispin, X. Optimization of the Thermoelectric Figure of Merit in the Conducting Polymer Poly (3, 4-Ethylenedioxythiophene). *Nat. Mater.* **2011**, *10*, 429−433.
(21) Kroon, R.; Mengistie, D. A.; Kiefer, D.; Hynynen, J.; Ryan, J. D.; Yu, L.; Müller, C. Thermoelectric Plastics: From Design to Synthesis, Processing and Structure−property Relationships. *Chem. Soc. Rev.* **2016**, *45*, 6147−6164.
(22) Russ, B.; Glaudell, A.; Urban, J. J.; Chabinyc, M. L.; Segalman, R. A. Organic Thermoelectric Materials for Energy Harvesting and Temperature Control. *Nat. Rev. Mater.* **2016**, *1*, 16050.
(23) Qi, Y.; Mohapatra, S. K.; Kim, S. B.; Barlow, S.; Marder, S. R.; Kahn, A. Solution Doping of Organic Semiconductors Using Air-Stable n-Dopants. *Appl. Phys. Lett.* **2012**, *100*, No. 083305.
(24) Lu, G.; Blakesley, J.; Himmelberger, S.; Pingel, P.; Frisch, J.; Lieberwirth, I.; Salzmann, I.; Oehzelt, M.; Di Pietro, R.; Salleo, A.; Koch, N.; Neher, D. Moderate Doping Leads to High Performance of Semiconductor/Insulator Polymer Blend Transistors. *Nat. Commun.* **2013**, *4*, 1588.
(25) Werner, A. G.; Li, F.; Harada, K.; Pfeiffer, M.; Fritz, T.; Leo, K. Pyronin B as a Donor for N-Type Doping of Organic Thin Films. *Appl. Phys. Lett.* **2003**, *82*, 4495−4497.
(26) Li, F.; Werner, A.; Pfeiffer, M.; Leo, K.; Liu, X. Leuco Crystal Violet as a Dopant for N-Doping of Organic Thin Films of Fullerene C60. *J. Phys. Chem. B* **2004**, *108*, 17076−17082.
(27) Werner, A.; Li, F.; Harada, K.; Pfeiffer, M.; Fritz, T.; Leo, K.; Machill, S. N-Type Doping of Organic Thin Films Using Cationic Dyes. *Adv. Funct. Mater.* **2004**, *14*, 255−260.
(28) Chueh, C.-C.; Li, C.-Z.; Ding, F.; Li, Z.; Cernetic, N.; Li, X.; Jen, A. K.-Y. Doping Versatile N-Type Organic Semiconductors via Room Temperature Solution-Processable Anionic Dopants. *ACS Appl. Mater. Interfaces* **2017**, *9*, 1136−1144.
(29) Lussem, B.; Riede, M.; Leo, K. Doping of Organic Semiconductors. *Phys. Status Solidi A* **2013**, *210*, 9−43.
(30) Bubnova, O.; Crispin, X. Environmental Science Towards Polymer-Based Organic Thermoelectric Generators. *Energy Environ. Sci.* **2012**, *5*, 9345.
(31) Kim, G.; Shao, L.; Zhang, K.; Pipe, K. P. Engineered Doping of Organic Semiconductors for Enhanced Thermoelectric Efficiency. *Nat. Mater.* **2013**, *12*, 719−723.
(32) Toshima, N. Conductive Polymers as a New Type OfThermoelectric Material. *Macromol. Symp.* **2002**, *186*, 81−86.
(33) Zhang, K.; Zhang, Y.; Wang, S. Enhancing Thermoelectric Properties of Organic Composites through Hierarchical Nanostructures. *Sci. Rep.* **2013**, *3*, 3448.
(34) Fan, Z.; Li, P.; Du, D.; Ouyang, J. Significantly Enhanced Thermoelectric Properties of PEDOT:PSS Films through Sequential Post-Treatments with Common Acids and Bases. *Adv. Energy Mater.* **2017**, *7*, 1602116.
(35) Cowen, L. M.; Atoyo, J.; Carnie, M. J.; Baran, D.; Schroeder, B. C. Review — Organic Materials for Thermoelectric Energy Generation. *ECS J. Solid State Sci. Technol.* **2017**, *6*, N3080−N3088.
(36) Tietze, M. L.; Rose, B. D.; Schwarze, M.; Fischer, A.; Runge, S.; Blochwitz-Nimoth, J.; Lüssem, B.; Leo, K.; Brédas, J. L. Passivation of Molecular N-Doping: Exploring the Limits of Air Stability. *Adv. Funct. Mater.* **2016**, *26*, 3730−3737.
(37) Naab, B. D.; Guo, S.; Olthof, S.; Evans, E. G. B.; Wei, P.; Millhauser, G. L.; Kahn, A.; Barlow, S.; Marder, S. R.; Bao, Z.

DOI: 10.1021/acsaem.8b00777
ACS Appl. Energy Mater. 2018, 1, 4626−4634

Mechanistic Study on the Solution-Phase n-Doping of 1,3-Dimethyl-2-Aryl-2,3-Dihydro-1H-Benzoimidazole Derivatives. *J. Am. Chem. Soc.* **2013**, *135*, 15018−15025.
(38) Schlitz, R. A.; Brunetti, F. G.; Glaudell, A. M.; Miller, P. L.; Brady, M. A.; Takacs, C. J.; Hawker, C. J.; Chabinyc, M. L. Solubility-Limited Extrinsic n-Type Doping of a High Electron Mobility Polymer for Thermoelectric Applications. *Adv. Mater.* **2014**, *26*, 2825−2830.
(39) Liu, J.; Qiu, L.; Portale, G.; Koopmans, M.; ten Brink, G.; Hummelen, J. C.; Koster, L. J. A. N-Type Organic Thermoelectrics: Improved Power Factor by Tailoring Host−Dopant Miscibility. *Adv. Mater.* **2017**, *29*, 1701641.
(40) Qiu, L.; Liu, J.; Alessandri, R.; Qiu, X.; Koopmans, M.; Havenith, R. W. A.; Marrink, S. J.; Chiechi, R. C.; Anton Koster, L. J.; Hummelen, J. C. Enhancing Doping Efficiency by Improving Host-Dopant Miscibility for Fullerene-Based n-Type Thermoelectrics. *J. Mater. Chem. A* **2017**, *5*, 21234−21241.
(41) Shi, K.; Zhang, F.; Di, C.-A.; Yan, T.-W.; Zou, Y.; Zhou, X.; Zhu, D.; Wang, J.-Y.; Pei, J. Toward High Performance n -Type Thermoelectric Materials by Rational Modification of BDPPV Backbones. *J. Am. Chem. Soc.* **2015**, *137*, 6979−6982.
(42) de Leeuw, D. M.; Simenon, M. M. J.; Brown, A. R.; Einerhand, R. E. F. Stability of N-Type Doped Conducting Polymers and Consequences for Polymeric Microelectronic Devices. *Synth. Met.* **1997**, *87*, 53−59.
(43) Jousselme, B.; Sonmez, G.; Wudl, F. Acidity and Electronegativity Enhancement of C 60 Derivatives through Cyano Groups. *J. Mater. Chem.* **2006**, *16*, 3478−3482.
(44) van der Boom, T.; Hayes, R. T.; Zhao, Y.; Bushard, P. J.; Weiss, E. A.; Wasielewski, M. R. Charge Transport in Photofunctional Nanoparticles Self-Assembled from Zinc 5,10,15,20-Tetrakis-(Perylenediimide)Porphyrin Building Blocks. *J. Am. Chem. Soc.* **2002**, *124*, 9582−9590.
(45) Di Pietro, R.; Fazzi, D.; Kehoe, T. B.; Sirringhaus, H. Spectroscopic Investigation of Oxygen- and Water-Induced Electron Trapping and Charge Transport Instabilities in n-Type Polymer Semiconductors. *J. Am. Chem. Soc.* **2012**, *134*, 14877.
(46) Jones, B. A.; Facchetti, A.; Wasielewski, M. R.; Marks, T. J. Tuning Orbital Energetics in Arylene Diimide Semiconductors. Materials Design for Ambient Stability of n-Type Charge Transport. *J. Am. Chem. Soc.* **2007**, *129*, 15259−15278.
(47) Naab, B. D.; Gu, X.; Kurosawa, T.; To, J. W. F.; Salleo, A.; Bao, Z. Role of Polymer Structure on the Conductivity of N-Doped Polymers. *Adv. Electron. Mater.* **2016**, *2*, 1600004.
(48) Zhang, Y.; Phan, H.; Zhou, H.; Zhang, X.; Zhou, J.; Moudgil, K.; Barlow, S.; Marder, S. R.; Facchetti, A.; Nguyen, T. Q. Electron Transport and Nanomorphology in Solution-Processed Polymeric Semiconductor n-Doped with an Air-Stable Organometallic Dimer. *Adv. Electron. Mater.* **2017**, *3*, 1600546.
(49) Yang, J.; Xiao, B.; Tajima, K.; Nakano, M.; Takimiya, K.; Tang, A.; Zhou, E. Comparison among Perylene Diimide (PDI), Naphthalene Diimide (NDI), and Naphthodithiophene Diimide (NDTI) Based n-Type Polymers for All-Polymer Solar Cells Application. *Macromolecules* **2017**, *50*, 3179−3185.
(50) Nakano, K.; Nakano, M.; Xiao, B.; Zhou, E.; Suzuki, K.; Osaka, I.; Takimiya, K.; Tajima, K. Naphthodithiophene Diimide-Based Copolymers: Ambipolar Semiconductors in Field-Effect Transistors and Electron Acceptors with Near-Infrared Response in Polymer Blend Solar Cells. *Macromolecules* **2016**, *49*, 1752−1760.
(51) Yang, J.; Chen, F.; Xiao, B.; Sun, S.; Sun, X.; Tajima, K.; Tang, A.; Zhou, E. Modulating the Symmetry of Benzodithiophene by Molecular Tailoring for the Application in Naphthalene Diimide-Based N-Type Photovoltaic Polymers. *Sol. RRL* **2018**, *2*, 1700230.
(52) Zhou, E.; Nakano, M.; Izawa, S.; Cong, J.; Osaka, I.; Takimiya, K.; Tajima, K. All-Polymer Solar Cell with High near-Infrared Response Based on a Naphthodithiophene Diimide (NDTI) Copolymer. *ACS Macro Lett.* **2014**, *3*, 872−875.
(53) Zhou, E.; Cong, J.; Hashimoto, K.; Tajima, K. Control of Miscibility and Aggregation via the Material Design and Coating Process for High-Performance Polymer Blend Solar Cells. *Adv. Mater.* **2013**, *25*, 6991−6996.
(54) Zhou, E.; Cong, J.; Wei, Q.; Tajima, K.; Yang, C.; Hashimoto, K. All-Polymer Solar Cells from Perylene Diimide Based Copolymers: Material Design and Phase Separation Control. *Angew. Chem., Int. Ed.* **2011**, *50*, 2799−2803.
(55) Bucella, S. G.; Luzio, A.; Gann, E.; Thomsen, L.; McNeill, C. R.; Pace, G.; Perinot, A.; Chen, Z.; Facchetti, A.; Caironi, M. Macroscopic and High-Throughput Printing of Aligned Nanostructured Polymer Semiconductors for MHz Large-Area Electronics. *Nat. Commun.* **2015**, *6*, 8394.
(56) Tilley, A. J.; Guo, C.; Miltenburg, M. B.; Schon, T. B.; Yan, H.; Li, Y.; Seferos, D. S. Thionation Enhances the Electron Mobility of Perylene Diimide for High Performance n -Channel Organic Field Effect Transistors. *Adv. Funct. Mater.* **2015**, *25*, 3321−3329.
(57) Chen, W.; Zhang, J.; Long, G.; Liu, Y.; Zhang, Q. From Non-Detectable to Decent: Replacement of Oxygen with Sulfur in Naphthalene Diimide Boosts Electron Transport in Organic Thin-Film Transistors. *J. Mater. Chem. C* **2015**, *3*, 8219−8224.
(58) Kozycz, L. M.; Guo, C.; Manion, J. G.; Tilley, A. J.; Lough, A. J.; Li, Y.; Seferos, D. S. Enhanced Electron Mobility in Crystalline Thionated Naphthalene Diimides. *J. Mater. Chem. C* **2015**, *3*, 11505−11515.
(59) Welford, A.; Maniam, S.; Gann, E.; Thomsen, L.; Langford, S. J.; Mcneill, C. R. Thionation of Naphthalene Diimide Molecules: Thin-Film Microstructure and Transistor Performance. *Org. Electron.* **2018**, *53*, 287−295.
(60) Pahlavanlu, P.; Tilley, A. J.; Mcallister, B. T.; Seferos, D. S. Microwave Synthesis of Thionated Naphthalene Diimide-Based Small Molecules and Polymers. *J. Org. Chem.* **2017**, *82*, 12337.
(61) Shin, Y.; Welford, A.; Komber, H.; Matsidik, R.; Thurn-Albrecht, T.; McNeill, C. R.; Sommer, M. Regioregular Polymer Analogous Thionation of Naphthalene Diimide − Bithiophene Copolymers. *Macromolecules* **2018**, *51*, 984−991.
(62) Luzio, A.; Fazzi, D.; Natali, D.; Giussani, E.; Baeg, K. J.; Chen, Z.; Noh, Y. Y.; Facchetti, A.; Caironi, M. Synthesis, Electronic Structure, and Charge Transport Characteristics of Naphthalenediimide-Based Co-Polymers with Different Oligothiophene Donor Units. *Adv. Funct. Mater.* **2014**, *24*, 1151−1162.
(63) Fazzi, D.; Caironi, M.; Castiglioni, C. Quantum-Chemical Insights into the Prediction of Charge Transport Parameters for a Naphthalenetetracarboxydiimide-Based Copolymer with Enhanced Electron Mobility. *J. Am. Chem. Soc.* **2011**, *133*, 19056−19059.
(64) Wang, S.; Sun, H.; Ail, U.; Vagin, M.; Persson, P. O. A.; Andreasen, J. W.; Thiel, W.; Berggren, M.; Crispin, X.; Fazzi, D.; Fabiano, S. Thermoelectric Properties of Solution-Processed n-Doped Ladder-Type Conducting Polymers. *Adv. Mater.* **2016**, *28*, 10764−10771.
(65) Shin, Y.; Massetti, M.; Komber, H.; Biskup, T.; Nava, D.; Lanzani, G.; Caironi, M.; Sommer, M. Improving Miscibility of a Naphthalene Diimide-Bithiophene Copolymer with n-Type Dopants through the Incorporation of "Kinked" Monomers. *Adv. Electron. Mater.* **2018**, *1*, 1700581.
(66) Kiefer, D.; Giovannitti, A.; Sun, H.; Biskup, T.; Hofmann, A.; Koopmans, M.; Cendra, C.; Weber, S.; Anton Koster, L. J.; Olsson, E.; Rivnay, J.; Fabiano, S.; McCulloch, I.; Müller, C. Enhanced N-Doping Efficiency of a Naphthalenediimide-Based Copolymer through Polar Side Chains for Organic Thermoelectrics. *ACS Energy Lett.* **2018**, *3*, 278−285.
(67) Garcia-belmonte, G.; Munar, A.; Barea, E. M.; Bisquert, J.; Ugarte, I.; Pacios, R. Charge Carrier Mobility and Lifetime of Organic Bulk Heterojunctions Analyzed by Impedance Spectroscopy. *Org. Electron.* **2008**, *9*, 847.
(68) Bittle, E. G.; Basham, J. I.; Jackson, T. N.; Jurchescu, O. D.; Gundlach, D. J. Mobility Overestimation Due to Gated Contacts in Organic Field-Effect Transistors. *Nat. Commun.* **2016**, *7*, 10908.
(69) Africa, P. C.; de Falco, C.; Maddalena, F.; Caironi, M.; Natali, D. Simultaneous Extraction of Density of States Width, Carrier

DOI: 10.1021/acsaem.8b00777
ACS Appl. Energy Mater. 2018, 1, 4626−4634

Mobility and Injection Barriers in Organic Semiconductors. *Sci. Rep.* **2017**, *7*, 3803.
(70) Lu, N.; Li, L.; Liu, M. A Review of Carrier Thermoelectric-Transport Theory in Organic Semiconductors. *Phys. Chem. Chem. Phys.* **2016**, *18*, 19503.
(71) Lilliu, S.; Agostinelli, T.; Pires, E.; Hampton, M.; Nelson, J.; Macdonald, J. E. Dynamics of Crystallization and Disorder during Annealing of P3HT/PCBM Bulk Heterojunctions. *Macromolecules* **2011**, *44*, 2725−2734.
(72) Kirby, N. M.; Mudie, S. T.; Hawley, A. M.; Cookson, D. J.; Mertens, H. D. T.; Cowieson, N.; Samardzic-Boban, V. A Low-Background-Intensity Focusing Small-Angle X-Ray Scattering Undulator Beamline. *J. Appl. Crystallogr.* **2013**, *46*, 1670−1680.
(73) Ilavsky, J. Nika: Software for Two-Dimensional Data Reduction. *J. Appl. Crystallogr.* **2012**, *45*, 324−328.
(74) Beretta, D.; Massetti, M.; Lanzani, G.; Caironi, M. Thermoelectric Characterization of Flexible Micro-thermoelectric Generators. *Rev. Sci. Instrum.* **2017**, *88*, No. 015103.

DOI: 10.1021/acsaem.8b00777
ACS Appl. Energy Mater. 2018, 1, 4626−4634